Local Mass Transfer Correlations for Nonaqueous Phase Liquid Pool Dissolution in Saturated Porous Media

CONSTANTINOS V. CHRYSIKOPOULOS and TAE-JOON KIM
Department of Civil and Environmental Engineering, University of California, Irvine, CA 92697–2175, U.S.A.; e-mail; costas@eng.uci.edu

Abstract. Local mass transfer correlations are developed to describe the rate of interface mass transfer of single component nonaqueous phase liquid (NAPL) pools in saturated subsurface formations. A three-dimensional solute transport model is employed to compute local mass transfer coefficients from concentration gradients at the NAPL–water interface, assuming that the aqueous phase concentration along the NAPL–water interface is constant and equal to the solubility concentration. Furthermore, it is assumed that the porous medium is homogeneous, the interstitial fluid velocity steady and the dissolved solute may undergo first-order decay or may sorb under local equilibrium conditions. Power-law expressions relating the local Sherwood number to appropriate local Peclet numbers are developed for both rectangular and elliptic/circular source geometries. The proposed power law correlations are fitted to numerically generated data and the correlation coefficients are determined using nonlinear least squares regression. The estimated correlation coefficients are found to be direct functions of the interstitial fluid velocity, pool dimensions, and pool geometry.

Key words: contaminant transport, NAPL pool dissolution, mass transfer correlations.

Abbreviations: NAPL – nonaqueous phase liquid, sse – sum of squared error.

Nomenclature

a	major semiaxis of elliptic pool [L].
b	minor semiaxis of elliptic pool [L].
C	aqueous phase solute concentration (solute mass/liquid volume) [M/L^3].
C_s	single component aqueous saturation concentration (solubility) [M/L^3].
$\mathcal{D}$	molecular diffusion coefficient [L^2/t].
$\mathcal{D}_e$	effective molecular diffusion coefficient, equal to $\mathcal{D}/\tau$, [L^2/t].
D_x, D_y, D_z	longitudinal, lateral and vertical hydrodynamic dispersion coefficients, respectively [L^2/t].
f	arbitrary function.
J	local mass flux from a NAPL pool [M/L^2/t].
k	local mass transfer coefficient [L/t].
$\widehat{k}$	time invariant local mass transfer coefficient [L/t].
K_d	partition coefficient (liquid volume/solid mass) [L^3/M].
ℓ_c	characteristic length [L].

ℓ_x, ℓ_y	pool dimensions in x and y directions, respectively [L].
ℓ_{x_0}, ℓ_{y_0}	x and y Cartesian coordinates, respectively, of the origin of a rectangular pool or the center of an elliptic/circular pool [L].
$Pe_{x(e)}, Pe_{y(e)}$	local Peclet numbers for elliptic/circular pools in x and y directions, defined in (26) and (27), respectively.
$Pe_{x(r)}, Pe_{y(r)}$	local Peclet numbers for rectangular pools in x and y directions, defined in (19) and (20), respectively.
R	dimensionless retardation factor.
$\mathcal{R}_{(e)}$	region defined by an elliptic NAPL–water interfacial area.
$\mathcal{R}_{(r)}$	region defined by a rectangular NAPL–water interfacial area.
$Sh_{(e)}$	local Sherwood number for an elliptic/circular NAPL pool.
$Sh_{(r)}$	local Sherwood number for a rectangular NAPL pool.
t	time, t.
U_x	average interstitial velocity [L/t].
x, y, z	spatial coordinates [L].
x', y'	shifted x and y Cartesian coordinates, respectively [L].

Greek Letters

$\alpha_L, \alpha_T, \alpha_V$	longitudinal, transverse and vertical dispersivities, respectively [L].
$\beta_1, \beta_2, \beta_3$	empirical coefficients.
$\gamma_1, \gamma_2, \gamma_3$	empirical coefficients.
θ	porosity.
λ	decay coefficient of the liquid phase concentration [t^{-1}].
λ^*	decay coefficient of the concentration sorbed onto the solid matrix [t^{-1}].
$\Pi_1, \ldots, \Pi_6$	dimensionless variables defined in (13)–(18).
ρ	bulk density of the solid matrix [M/L^3].
τ	tortuosity.
ϕ	arbitrary function.

1. Introduction

Groundwater contamination by nonaqueous phase liquids (NAPLs) originating from industrial and commercial activities currently is recognized as an important world-wide problem. Most of the NAPLs are organic solvents and petroleum hydrocarbons originating from leaking underground storage tanks, ruptured pipelines, surface spills, hazardous waste landfills, and disposal sites. As a NAPL is released into the subsurface environment, it infiltrates through the vadose zone leaving behind blobs or ganglia which are no longer connected to the main body of the organic liquid (Geller and Hunt, 1993; Seagren *et al.*, 1993). Upon reaching the water table NAPLs lighter than water remain above the water table in the form of a floating pool; NAPLs heavier than water continue to migrate downward until they encounter an impermeable layer where a flat pool starts to form (Seagren *et al.*, 1994; Chrysikopoulos, 1995). As groundwater flows past trapped ganglia or NAPL pools, a plume of dissolved hydrocarbons is created.

The concentration of a dissolved NAPL in groundwater is governed mainly by interface mass-transfer processes that often are slow and rate-limited (Mackay *et al.*, 1985; Powers *et al.*, 1991). There is a relatively large body of available

literature on the migration of NAPLs and dissolution of residual blobs as well as lenses (Schwille, 1988; Celia *et al*., 1993; Lenhard *et al*., 1993; Illangasekare *et al*., 1995; Bear *et al*., 1996; Demond *et al*., 1996; Keller *et al*., 1997; Kennedy and Lennox, 1997), and pools (Anderson *et al*., 1992; Johnson and Pankow, 1992; Chrysikopoulos *et al*., 1994; Voudrias and Yeh, 1994; Lee and Chrysikopoulos, 1995, 1998; Holman and Javandel, 1996; Mason and Kueper, 1996; Chrysikopoulos and Lee, 1998). Furthermore, empirical correlations useful for convenient estimation of NAPL dissolution rates, expressed in terms of non-dimensional parameters, for well-defined residual blobs are available in the literature (Miller *et al*., 1990; Parker *et al*., 1991; Powers *et al*., 1992; Imhoff *et al*., 1993). These correlations relate the Reynolds number and NAPL volumetric fraction to the dimensionless mass transfer rate coefficient (Sherwood number), and differ mainly in the number and type of dimensionless system properties accounted for (Mayer and Miller, 1996). The existing correlations indicate that dissolution rates for residual NAPLs in one-dimensional soil columns are highly dependent on blob shape and size, interstitial velocity, and/or length of soil zone exposed to residual NAPLs (Powers *et al*., 1991; Imhoff *et al*., 1993).

Mass transfer correlations applicable to NAPL pool dissolution in porous media have not been established yet. It should be noted that NAPL pool dissolution is substantially different than residual NAPL dissolution, owing primarily to different source geometries. For the case of dissolving flat volatile solids or liquids in the presence of laminar gas flow, appropriate mass transfer correlations have been developed by solving the governing boundary layer equations and assuming that mass transfer occurs only by convection in the flow direction (Incropera and DeWitt, 1990; Bird *et al*., 1960). However, for NAPL pool dissolution in subsurface formations dispersion effects can not be ignored.

In this paper, local mass transfer correlations for the rate of interface mass transfer of single component NAPL pools are developed for both rectangular and elliptic/circular NAPL pool geometries. Power-law relationships are used to relate the dimensionless local mass transfer coefficients with the appropriate local Peclet numbers. The impact of groundwater velocity, pool size, and pool geometry on mass transfer rates associated with NAPL pool dissolution is investigated.

2. Background

Several mathematical models describing the dissolution of residual NAPLs in porous media employ the assumption that the dissolved concentration along the NAPL–water interface is equal to the solubility or aqueous saturation concentration (Pinder and Abriola, 1986; Holman and Javandel, 1996). Results from many experimental column studies associated with residual NAPL dissolution support the applicability of this assumption (Miller *et al*., 1990; van der Waarden *et al*., 1971; Fried *et al*., 1979; Borden and Kao, 1992; Borden and Piwoni, 1992). However, significant deviations from thermodynamic equilibrium have been observed

for high groundwater velocities and certain blob shapes, sizes and distributions (Schwille *et al.*, 1975; Mackay *et al.*, 1985). Interface mass transfer limitations often are attributed to preferential groundwater flow and aquifer heterogeneities (Wilson *et al.*, 1988; Mayer and Miller, 1996).

Generally, NAPL pools tend to be continuous and nearly saturated zones with relatively small vertical thickness. Also, the vertical distances covered by the dissolved NAPL plumes are often assumed smaller than the vertical scale of aquifer heterogeneity; therefore, the aquifer zone in the vicinity of a dissolving NAPL pool may be considered as a relatively homogeneous porous formation (Johnson and Pankow, 1992). Furthermore, for typical groundwater velocities, a boundary condition specifying a constant aqueous saturation concentration at the NAPL–water interface may be considered valid (Johnson and Pankow, 1992; Seagren *et al.*, 1994). Under such idealized conditions it is possible to estimate local mass transfer coefficients applicable at NAPL–water interfaces.

For a NAPL pool with uniform pool-water interface and insignificant thickness relative to the thickness of the aquifer, the interface mass flux controlled by effective molecular diffusion is adequately equated by a single-resistance, linear-driving force model as follows (Chrysikopoulos, 1995)

$$J(t, x, y) = -\mathcal{D}_e \frac{\partial C(t, x, y, 0)}{\partial z} = k(t, x, y)[C_s - C(t, x, y, \infty)], \qquad (1)$$

where $J(t, x, y)$ is the local mass flux perpendicular to the NAPL pool; $C(t, x, y, z)$ is the liquid phase contaminant concentration; C_s is the aqueous concentration at the interface and for a pure organic liquid equals the liquid's aqueous saturation (solubility) concentration; $\mathcal{D}_e = \mathcal{D}/\tau$ is the effective aqueous diffusion coefficient in the porous medium (where $\mathcal{D}$ is the molecular diffusion coefficient; and $\tau \geqslant 1$ is the tortuosity coefficient); $k(t, x, y)$ is the local mass transfer coefficient dependent on time and location on the NAPL–water interface; x, y, z are the spatial coordinates in the longitudinal, lateral, and vertical directions, respectively; and t is time. It should be noted that the NAPL–water interface is located at $z = 0$, and $z \to \infty$ corresponds to any location above the concentration boundary layer (see Figure 1). Therefore, $C(t, x, y, \infty) = C_\infty$ represents the bulk contaminant concentration outside the boundary layer. The relationship (1) implies that at the interface there is no fluid motion and mass transfer occurs only by effective molecular diffusion. The local mass transfer coefficient is physically proportional to the gradient of the contaminant concentration at the NAPL–water interface and is obtained from (1) as follows:

$$k(t, x, y) = \frac{-\mathcal{D}_e}{C_s - C(t, x, y, \infty)} \frac{\partial C(t, x, y, 0)}{\partial z}. \qquad (2)$$

The time required for complete pool dissolution is much longer than the contact time between the pool and the flowing groundwater (Johnson and Pankow, 1992; Seagren *et al.*, 1994). Therefore, in this work local mass transfer coefficients are es-
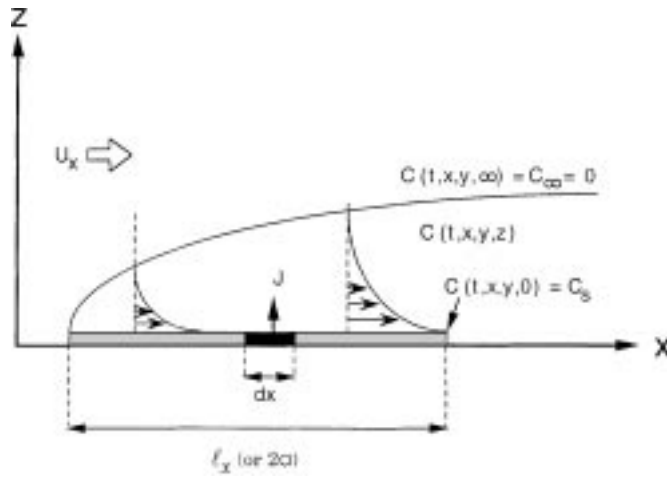
Figure 1. Schemetic illustration of a crossection of the NAPL pool and dissolved concentration boundary layer showing the unidirectional groundwater velocity U_x and the perpendicular to the pool surface local mass flux. Arrows are used for convenient sketching of the magnitude of the scalar concentration within the boundary layer.

timated at steady-state conditions. The time invariant local mass transfer coefficient is denoted by $\widehat{k}(x, y)$.

3. Model Development

3.1. MODEL FORMULATION

The transient contaminant transport from a dissolving NAPL pool denser than water in a three-dimensional, homogeneous porous medium under steady-state uniform flow conditions, assuming that the dissolved organic is sorbing under local equilibrium conditions, is governed by the following partial differential equation (Chrysikopoulos, 1995):

$$
\begin{aligned}
R\frac{\partial C(t, x, y, z)}{\partial t} \;=\; & D_x\frac{\partial^2 C(t, x, y, z)}{\partial x^2} + \\
& + D_y\frac{\partial^2 C(t, x, y, z)}{\partial y^2} + D_z\frac{\partial^2 C(t, x, y, z)}{\partial z^2} \\
& - U_x\frac{\partial C(t, x, y, z)}{\partial x} - \lambda C(t, x, y, z) - \\
& - \lambda^*\frac{\rho}{\theta}K_d C(t, x, y, z),
\end{aligned}
\tag{3}
$$

where U_x is the average unidirectional interstitial fluid velocity; $R = 1 + K_d\rho/\theta$ is the dimensionless retardation factor for linear, reversible, instantaneous sorption; λ is the first-order decay constant of the liquid phase concentration; λ^* is the first-order decay coefficient of the concentration sorbed onto the solid matrix; K_d is
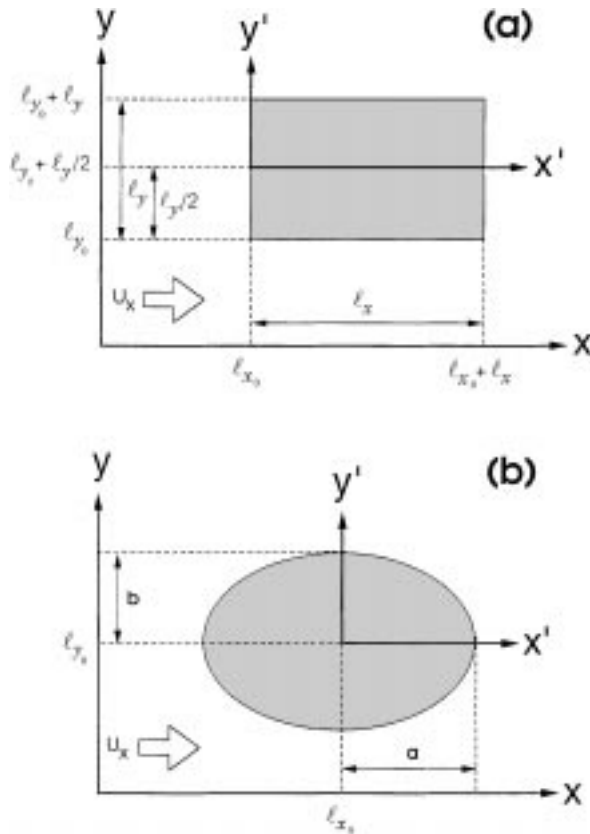
Figure 2. Plan view at $z = 0$ of (a) a rectangular NAPL pool with dimensions $\ell_x \times \ell_y$, and (b) an elliptic NAPL pool with origin at $x = \ell_{x_0}$, $y = \ell_{y_0}$, having major semiaxis a and minor semiaxis b. The primed spatial coordinates represent a shifted Cartesian coordinate system.

the partition or distribution coefficient; ρ is the bulk density of the solid matrix; θ is the porosity of the porous medium; D_x, D_y, D_z are the longitudinal, transverse, and vertical hydrodynamic dispersion coefficients, respectively, defined as (Bear and Verruijt, 1987)

$$D_x = \alpha_L U_x + \mathcal{D}_e, \tag{4a}$$

$$D_y = \alpha_T U_x + \mathcal{D}_e, \tag{4b}$$

$$D_z = \alpha_V U_x + \mathcal{D}_e, \tag{4c}$$

where α_L, α_T and α_V are the longitudinal, transverse and vertical dispersivities, respectively. For the special case where λ is equal to λ^*, the two decay terms in (3) are replaced by the term $\lambda R C$.

For a rectangular-shaped stagnant NAPL pool, as shown in Figure 2(a), the appropriate initial and boundary conditions are

$$C(0, x, y, z) = 0, \tag{5}$$

$$C(t, \pm\infty, y, z) = 0, \tag{6}$$

$$C(t, x, \pm\infty, z) = 0, \tag{7}$$

$$C(t, x, y, 0) = C_s, \qquad x, y \in \mathcal{R}_{(\mathrm{r})}, \tag{8a}$$

$$\frac{\partial C(t, x, y, 0)}{\partial z} = 0, \qquad x, y \notin \mathcal{R}_{(\mathrm{r})}, \tag{8b}$$

$$C(t, x, y, \infty) = 0, \tag{9}$$

where $\mathcal{R}_{(\mathrm{r})}$ is the domain defined by the rectangular NAPL–water interfacial area ($\ell_{x_0} \leqslant x \leqslant \ell_{x_0} + \ell_x$, $\ell_{y_0} \leqslant y \leqslant \ell_{y_0} + \ell_y$, where ℓ_{x_0} and ℓ_{y_0} indicate the x and y Cartesian coordinates of the pool origin, respectively; ℓ_x and ℓ_y are the pool dimensions in x and y directions, respectively). Equation (8a) implies that the aqueous concentration is constant over the pool and that the NAPL is in equilibrium with the water at the interface. Equation (9) represents the contaminant concentration outside the boundary layer which in this study is assumed to be zero.

For a NAPL pool of elliptic shape, as shown in Figure 2(b), the appropriate source boundary condition is

$$C(t, x, y, 0) = C_s, \qquad x, y \in \mathcal{R}_{(\mathrm{e})}, \tag{10a}$$

$$\frac{\partial C(t, x, y, 0)}{\partial z} = 0, \qquad x, y \notin \mathcal{R}_{(\mathrm{e})}, \tag{10b}$$

where $\mathcal{R}_{(\mathrm{e})}$ is the domain defined by an elliptic pool-water interfacial area ($(x - \ell_{x_0})^2/a^2 + (y - \ell_{y_0})^2/b^2 \leqslant 1$, where a and b are the major and minor semiaxes of the elliptic pool, respectively). Because a circular pool with radius r is just a special case of an elliptic pool, the appropriate source boundary condition for a circular pool is obtained by setting $a = b = r$.

3.2. NUMERICAL SOLUTION

The three-dimensional mathematical model presented by equations (3), (5)–(10) is solved numerically by an alternating direction implicit (ADI) finite-difference scheme. The ADI algorithm for three-dimensional transient partial differential equations is unconditionally stable (Huyakorn and Pinder, 1983). Furthermore, the ADI algorithm leads to a set of algebraic equations that form a tridiagonal matrix which may be solved by the highly efficient Thomas algorithm (Wang and Anderson, 1982).

Numerical simulations are performed to estimate profiles of aqueous phase concentrations for various interstitial velocities, pool dimensions and pool geometries. A zero flux boundary condition is applied to all outer boundaries of the numerical domain, and a constant boundary condition (8a) or (10a) is applied at the

pool-water interface. Time and space discretization is performed. Furthermore, appropriate dimensionless nodal separation distances are selected to avoid numerical oscillations (Hoffman, 1992; Schincariol *et al.*, 1994). It should be noted that the numerical codes developed here were consistently run until the simulated dissolved concentration profiles were no longer time dependent, because the desired local mass transfer coefficients should correspond to steady-state conditions.

4. Formulation of Mass Transfer Correlations

4.1. PROCEDURES AND ASSUMPTIONS

The interstitial fluid velocities employed for the model simulations presented in this work are 0.5, 0.7, 0.85 and 1.0 m/day, because solubility concentrations may occur at a NAPL–water interface when interstitial fluid velocities are less than 1.0 m/day (Powers *et al.*, 1991). Over 200 different rectangular pools with dimensions $\ell_x \times \ell_y$ in the range from 0.2 m × 0.2 m to 10.0 m × 10.0 m and approximately the same number of elliptic/circular pools with semiaxes $a \times b$ in the range 0.1 m × 0.1 m to 5.0 m × 5.0 m are examined. Local mass transfer coefficients are evaluated from numerical simulations based on various hydrodynamic conditions, pool sizes and pool shapes. Assuming that a plane of symmetry along the centerline of the pool in the downstream direction exists, local mass transfer coefficients are determined only for the top half of the NAPL–water interface.

For a NAPL pool located on top of an impermeable formation, a concentration boundary layer is developed above the NAPL–water interface. The thickness of the concentration boundary layer is mainly controlled by the contact time of groundwater with the NAPL–water interface which is directly affected by the interstitial groundwater velocity, hydrodynamic dispersion, and pool size. For uniform groundwater flow, the velocity boundary layer is ignored. Therefore, it is expected that fluid properties such as dynamic viscosities and densities for both groundwater and NAPL do not contribute to the formation of the concentration boundary layer. Furthermore, the bulk contaminant concentration outside the boundary layer is assumed to be zero, $C(t, x, y, \infty) = C_\infty = 0$, in the absence of residual NAPL ganglia trapped above the pool. Consequently, the local mass transfer coefficient (2) becomes independent of the saturation concentration, C_s, because $C(t, x, y, z)$ is a linear function of C_s (Chrysikopoulos *et al.*, 1994; Chrysikopoulos, 1995). Finally, the general mass transfer relationships are established by dimensional analysis with application of the Buckingham Pi theorem (Bird *et al.*, 1960; Perry *et al.*, 1984; Weber and DiGiano, 1996) and are expected to be independent of C_s.

4.2. RECTANGULAR POOL

The fundamental parameters that affect mass transfer from a single component rectangular NAPL pool are the interstitial fluid velocity, effective molecular diffusion, dispersion coefficients, local coordinates representing a specific location at

the NAPL–water interface, and the square root of the pool area (ℓ_c). The parameter ℓ_c is introduced to define the square root of a rectangular pool area, $(\ell_x\ell_y)^{1/2}$, and represents a characteristic length. For mathematical convenience, the origin of the Cartesian coordinate system used in this work is located at the center of the upgradient edge of the rectangular pool as shown in Figure 2(a). With respect to the shifted coordinate system, the coordinates x and y are expressed as $x' = x - \ell_{x_0}$ and $y' = y - (\ell_{y_0} + \ell_y/2)$. The time invariant local mass transfer coefficient for a single component rectangular NAPL pool can be represented by the following functional relationship:

$$\widehat{k}(x', y') = f(U_x, \mathcal{D}_e, D_x, D_y, x', y', \ell_c), \tag{11}$$

where f is an arbitrary function. There are eight dimensional variables in (11) and their fundamental dimensions are length (L) and time (t). Therefore, the necessary number of dimensionless groups needed to characterize the overall mass transfer coefficient is six. The relationship (11) can be rearranged to yield

$$\phi(\Pi_1, \Pi_2, \ldots, \Pi_6) = 0, \tag{12}$$

where each Π is an independent dimensionless product of some of the dimensional variables of the system considered, and ϕ is an arbitrary function. Dimensional analysis yields the following Π terms:

$$\Pi_1 = \frac{\widehat{k}(x', y')}{U_x}, \tag{13}$$

$$\Pi_2 = \frac{D_x}{\mathcal{D}_e}, \tag{14}$$

$$\Pi_3 = \frac{D_y}{\mathcal{D}_e}, \tag{15}$$

$$\Pi_4 = \frac{U_x x'}{\mathcal{D}_e}, \tag{16}$$

$$\Pi_5 = \frac{U_x y'}{\mathcal{D}_e}, \tag{17}$$

$$\Pi_6 = \frac{U_x \ell_c}{\mathcal{D}_e}. \tag{18}$$

Note that the local Peclet numbers, $\text{Pe}_{x(r)}$ and $\text{Pe}_{y(r)}$, that represent the advective–dispersive mass transfer in the x and y directions, respectively, can be obtained from the following combinations of Π terms:

$$\text{Pe}_{x(r)} = \frac{\Pi_4}{\Pi_2} = \frac{U_x x'}{D_x}, \tag{19}$$

$$\text{Pe}_{y(r)} = \frac{\Pi_5}{\Pi_3} = \frac{U_x y'}{D_y}, \tag{20}$$

where the subscript (r) designates a rectangular pool. Similarly, the Sherwood number, $\text{Sh}_{(r)}$, defined as the rate of interface mass transfer resistance to molecular diffusion resistance which physically represents the dimensionless concentration gradient at the NAPL–water interface can be expressed by the following relationship of Π terms:

$$\text{Sh}_{(r)} = \Pi_1 \Pi_6 \left(\frac{x' y'}{\ell_c^2} \right) = \frac{\widehat{k}(x', y') x' y'}{\mathcal{D}_e \ell_c}. \tag{21}$$

In view of (12) and (19)–(21) a proposed relationship for the local Sherwood number for a rectangular NAPL pool under uniform flow conditions is given by

$$\text{Sh}_{(r)}(x', y') = \beta_1 \text{Pe}_{x(r)}^{\beta_2} \text{Pe}_{y(r)}^{\beta_3}, \tag{22}$$

where β_1, β_2, and β_3 are empirical coefficients to be determined. The preceding equation is the general form of the desired mass transfer correlation expressed in the form of a power-law model consisting of two directional Peclet numbers and a leading coefficient. The coefficients β_1, β_2 and β_3 are estimated by fitting (22) to Sherwood numbers evaluated numerically by (21) where $\widehat{k}(x', y')$ is determined by the steady state version of (2) for various hydrodynamic conditions. In this work, parameter estimation is obtained by the nonlinear least squares regression routine RNLIN (IMSL, 1991). It should be noted that unlike overall Sherwood number correlations with constant coefficients which are often published in the literature, (22) is a proposed empirical relationship for the local Sherwood number. Therefore, the local empirical coefficients are expected to depend on pool geometry and hydrodynamic conditions.

The behavior of the local Sherwood number, $\text{Sh}_{(r)}$, as a function of x' and y' for a rectangular 2.5 m × 5 m, single component TCE pool ($\mathcal{D}_e = 2.43 \times 10^{-6} \, \text{m}^2/\text{h}$) in a homogeneous, saturated aquifer with interstitial velocity $U_x = 1.0 \, \text{m/d}$ is illustrated in Figure 3. The symbols (circles) represent numerically determined values whereas the solid lines represent the best fits obtained by correlation (22). The fitted coefficients are $\beta_1 = 0.03$, $\beta_2 = 0.68$ and $\beta_3 = 0.79$; furthermore, the corresponding residual sums of squared error (sse) are 1.08 and 2.25 for Figure 3(a) and Figure 3(b), respectively. Clearly, the numerically determined and fitted local Sherwood numbers are in very good agreement over the range considered of both x' (Figure 3(a)) and y' (Figure 3(b)). It should be noted that only the top half of the NAPL–water interface is considered here because of the assumed symmetry.

The dependence of the leading coefficient β_1 on ℓ_x and ℓ_y for four different velocities is illustrated in Figure 4. It is shown that the coefficient β_1 decreases with increasing ℓ_x (see Figure 4(a)), and increases almost linearly with increasing $\ell_y/2$ (see Figure 4(b)). Furthermore, β_1 decreases with increasing interstitial flow velocity U_x. Similarly, the dependence of the exponent β_2 associated with $\text{Pe}_{r(x)}$ on
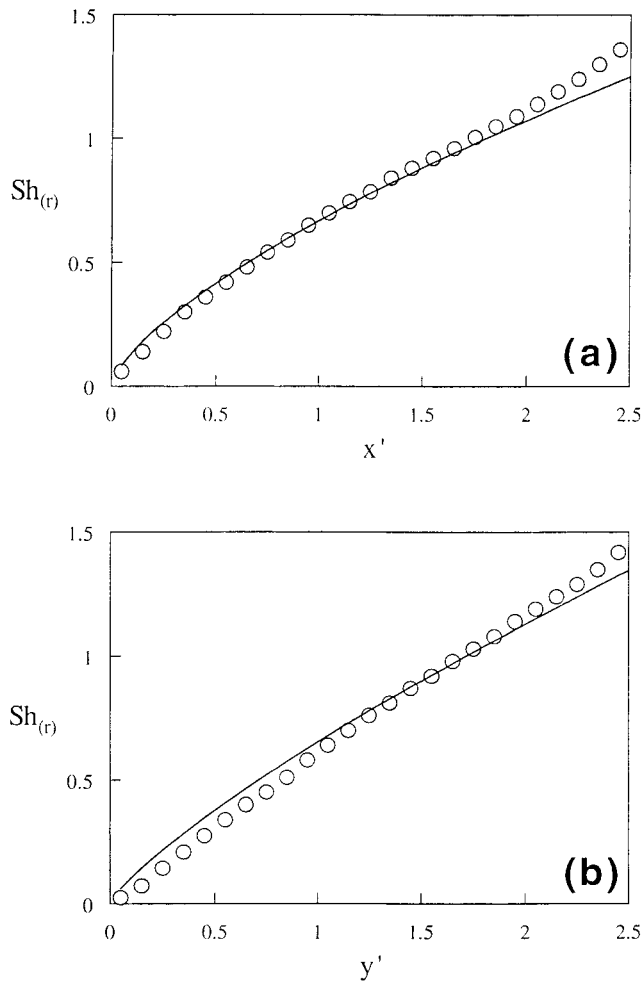
Figure 3. Comparison of numerically determined local Sherwood numbers for a rectangular pool (circles) and best correlation fits (solid curves) as a function of (a) x' with $y' = 1.30$ m and (b) y' with $x' = 1.30$ m.

ℓ_x and U_x is presented in Figure 5(a), and the dependence of β_3 associated with $Pe_{r(y)}$ on $\ell_y/2$ and U_x is shown in Figure 5(b). It should be noted that the exponent β_2 is independent of ℓ_y and proportional to U_x and ℓ_x. Furthermore, the exponent β_3 is independent of ℓ_x and almost insensitive to velocity changes and inversely proportional to $\ell_y/2$.

Using nonlinear regression analysis the numerically determined coefficients presented in Figures 4 and 5 (symbols) can be fitted by power-law functions of ℓ_x, $\ell_y/2$ and/or U_x (solid curves). The proposed functional relationships for the coefficients β_1, β_2, and β_3 are the following:

$$\beta_1 = 0.01 \, \ell_x^{-0.53} (\ell_y/2)^{1.16} \, U_x^{-0.11}, \tag{23}$$
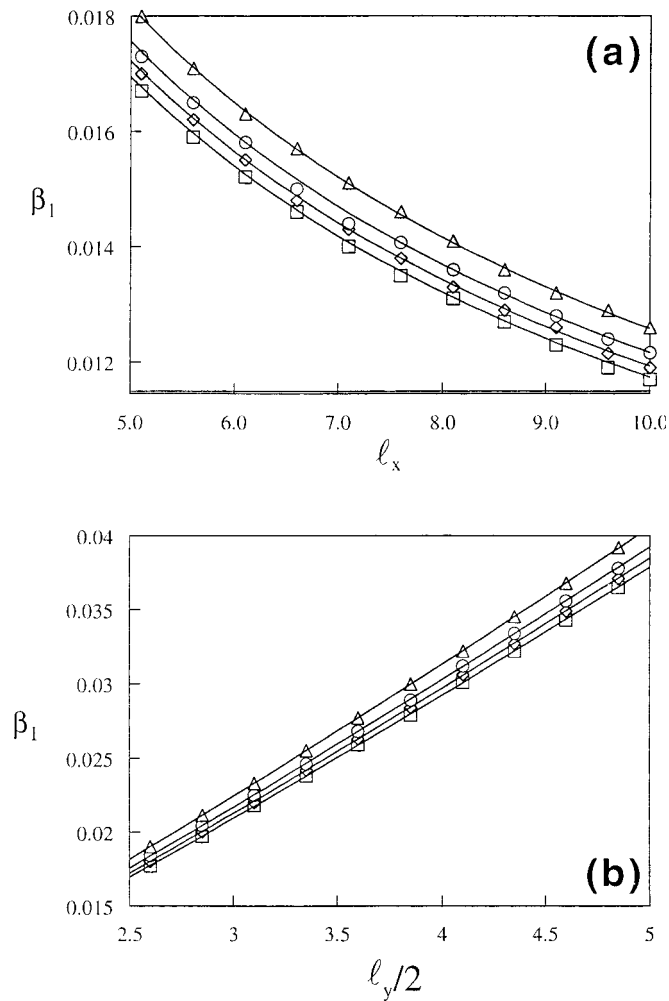
Figure 4. Variation of β_1 as a function of (a) ℓ_x with $\ell_y = 5.0$ m and (b) $\ell_y/2$ with $\ell_x = 5.0$ m for a rectangular NAPL pool with $U_x = 0.5$ m/d (triangles), 0.7 m/d (circles), 0.85 m/d (diamonds) and 1.0 m/d (squares). Symbols represent numerically determined coefficients and solid curves fitted power-law functions.

$$\beta_2 = 0.69 \, \ell_x^{0.13} \, U_x^{0.04}, \tag{24}$$

$$\beta_3 = 1.35 \, (\ell_y/2)^{-0.55} \, U_x^{0.01}. \tag{25}$$

It should be noted that only one half of the pool dimension in the y direction is used for the description of both β_1 and β_3, because of the assumed symmetry of the mass transfer coefficient distribution at the NAPL–water interface with respect to the pool centerline along the flow direction. The magnitude of each exponent is proportional to the rate of change of the coefficient with respect to changes in the corresponding system property. The expressions (23)–(25) are valid for groundwater
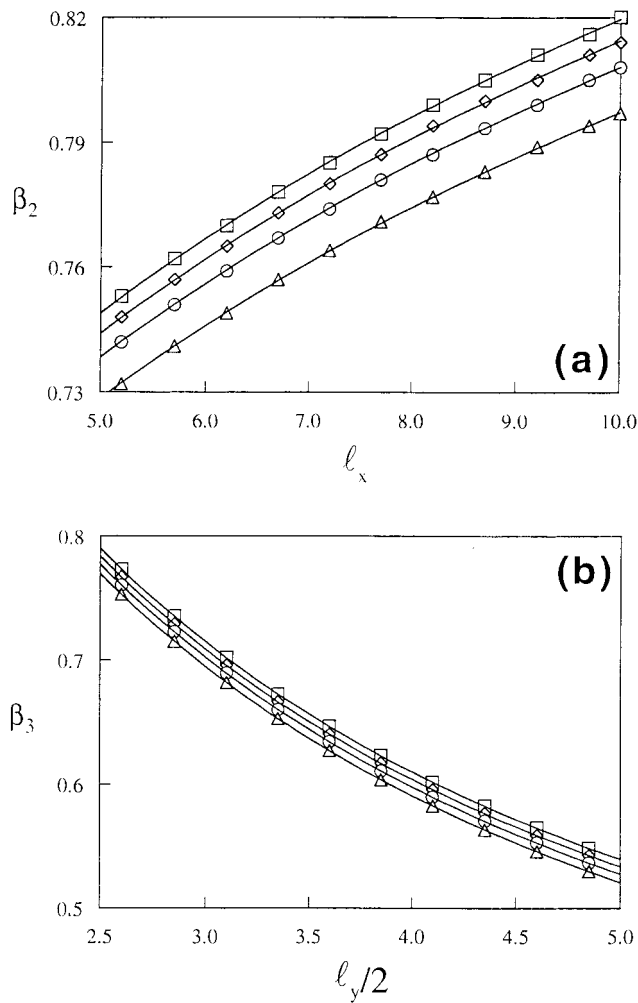
Figure 5. Variation of (a) β_2 as a function of ℓ_x and (b) β_3 as a function of $\ell_y/2$ for a rectangular NAPL pool with $U_x = 0.5$ m/d (triangles), 0.7 m/d (circles), 0.85 m/d (diamonds) and 1.0 m/d (squares). Symbols represent numerically determined coefficients and solid curves fitted power-law functions.

velocities in the range from 0.1 to 1.0 m/d and rectangular pools with dimensions $\ell_x \times \ell_y$ in the range from 0.2 m × 0.2 m to 10.0 m × 10.0 m.

4.3. ELLIPTIC/CIRCULAR POOL

For a single component elliptic/circular NAPL pool the fundamental parameters that affect the local mass transfer coefficient are the same as those listed for the case of a rectangular pool. For this case the characteristic length ℓ_c for an elliptic/circular pool is given by $(\pi ab)^{1/2}$. Also, the origin of the Cartesian coordin-

ate system is shifted to the center of the elliptic/circular pool as shown in Figure 2(b). With respect to the shifted coordinate system, the local coordinates x and y are expressed as $x' = x - \ell_{x_0}$ and $y' = y - \ell_{y_0}$. Furthermore, numerical simulations suggest that for an elliptic/circular NAPL pool in a homogeneous, saturated aquifer under ideal hydrodynamic conditions the local mass transfer coefficient is higher around the periphery than the center of the pool and relatively symmetric with respect to the pool center. Therefore, for mathematical convenience the variable x' is replaced by its absolute value $|x'|$.

Following the dimensional analysis outlined in the previous section, the x and y directional local Peclet numbers and the local Sherwood number for an elliptic/circular NAPL pool are formulated as follows:

$$\text{Pe}_{x(e)} = \frac{U_x |x'|}{D_x}, \tag{26}$$

$$\text{Pe}_{y(e)} = \frac{U_x y'}{D_y}, \tag{27}$$

$$\text{Sh}_{(e)} = \frac{\widehat{k}(x', y')|x'|y'}{\mathcal{D}_e \ell_c}, \tag{28}$$

where the subscript (e) designates an elliptic/circular pool, and $|x'|$ is the absolute value of the distance from the center of the pool along the flow direction. The proposed relationship for the local Sherwood number for an elliptic/circular NAPL pool is given by

$$\text{Sh}_{(e)}(x', y') = \gamma_1 \text{Pe}_{x(e)}^{\gamma_2} \text{Pe}_{y(e)}^{\gamma_3}, \tag{29}$$

where γ_1, γ_2 and γ_3 are empirical coefficients to be determined.

A comparison of $\text{Sh}_{(e)}$ values obtained by (28) (circles) and $\text{Sh}_{(e)}$ values determined with the local correlation (29) (solid curves) is presented in Figure 6 for a circular TCE pool ($a = b = r = 2.5$ m) in a homogeneous, saturated aquifer with interstitial velocity $U_x = 1.0$ m/d. The fitted coefficients are $\gamma_1 = 0.005$, $\gamma_2 = 3.46$ and $\gamma_3 = 3.51$; furthermore, the corresponding residual sums of squared error (sse) are 7.53 and 3.88 for Figure 6(a) and Figure 6(b), respectively. Good agreement is observed between the numerically determined and fitted local Sherwood numbers.

The dependence of the leading coefficient γ_1 on $2a$, b and U_x is illustrated in Figure 7. It is shown that γ_1 decreases with increasing $2a$, b and/or U_x. Changes in $2a$ and b have greater influence on γ_1 at lower velocities. The relationship of γ_2 and γ_3 as a function of $2a$, b and U_x are also presented in Figures 8 and 9, respectively. Clearly, both γ_2 and γ_3 increase with increasing $2a$ and U_x, and decreasing b. It should be noted that γ_3 is much more sensitive than β_3 to U_x because of pool geometry differences (compare Figures 5(b) and 9). The local mass transfer coefficient decreases with increasing distance from the front end of the NAPL pool, and has a maximum value at the leading or upstream edge where the impact of U_x is most
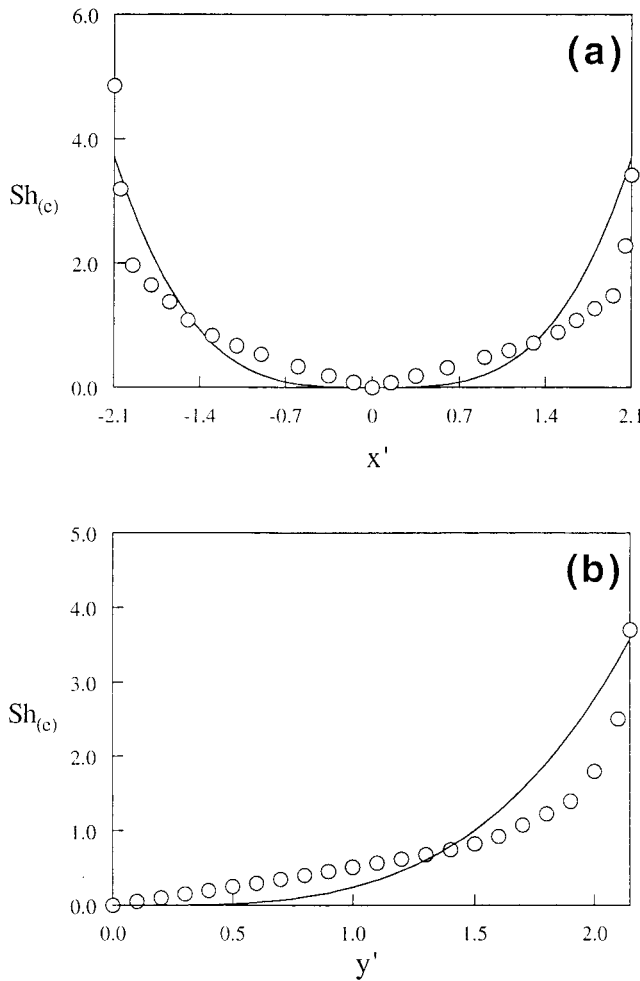
Figure 6. Comparison of numerically determined local Sherwood numbers for a circular NAPL pool (circles) and best correlation fits (solid curves) as a function of (a) x' with $y' = 1.25$ m and (b) y' with $x' = 1.20$ m.

pronounced. For a rectangular pool, the leading edge is perpendicular to U_x; therefore, changes in U_x can not affect considerably the $\widehat{k}(x, y)$ along the y direction. However, for an elliptic/circular NAPL pool the leading edge is a function of y and consequently, U_x fluctuations may have a strong impact on $\widehat{k}(x, y)$ along the y direction.

Using nonlinear regression analysis the numerically determined coefficients presented in Figures 7, 8 and 9 (symbols) can be fitted by appropriate power-law functions of $2a$, b and U_x. The proposed functional relationships for the coefficients γ_1, γ_2, and γ_3 are the following:

$$\gamma_1 = 0.10(2a)^{-3.26}b^{-1.51}U_x^{-1.21}, \tag{30}$$
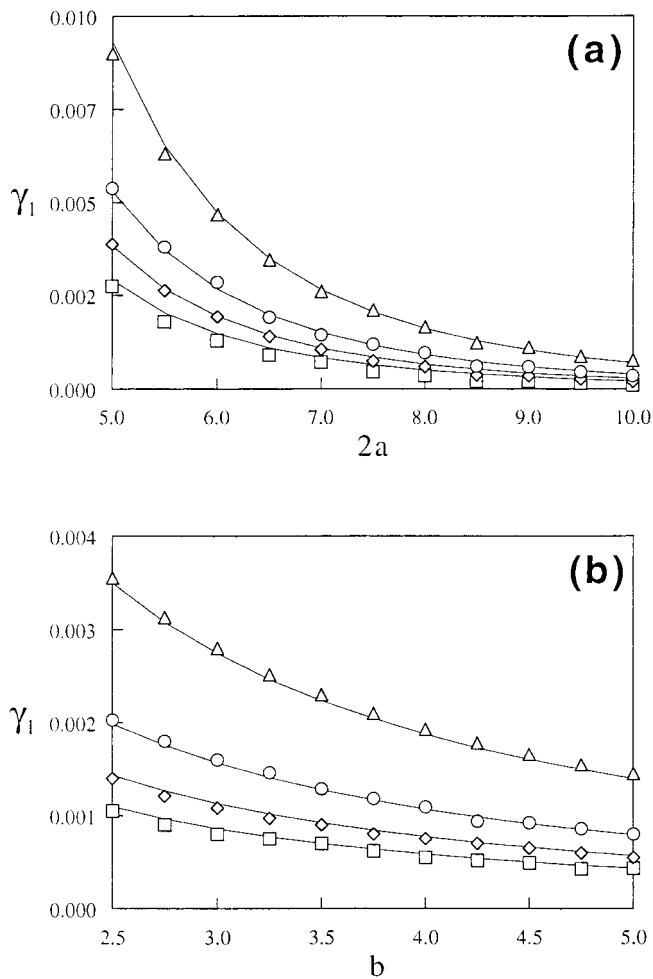
Figure 7. Variation of γ_1 as a function of (a) $2a$ with $b = 5.0$ m and (b) b with $a = 5.0$ m for an elliptic/circular pool with $U_x = 0.5$ m/d (triangles), 0.7 m/d (circles), 0.85 m/d (diamonds) and 1.0 m/d (squares). Symbols represent numerically determined coefficients and solid curves fitted power-law functions.

$$\gamma_2 = 5.31(2a)^{0.27} b^{-0.20} U_x^{0.21}, \tag{31}$$

$$\gamma_3 = 7.65(2a)^{0.10} b^{-0.19} U_x^{0.24}. \tag{32}$$

Unlike the coefficients β_2 and β_3 associated with the local Sherwood number correlation for rectangular NAPL pools (22) which require only two fitting parameters, both γ_2 and γ_3 involve three fitting parameters (i.e. $2a$, b, and U_x). It should be noted that the expressions (30)–(32) are valid for groundwater velocities in the range from 0.1 to 1.0 m/d and elliptic/circular NAPL pools with semiaxes $a \times b$ in the range from 0.1 m $\times$ 0.1 m to 5.0 m $\times$ 5.0 m.
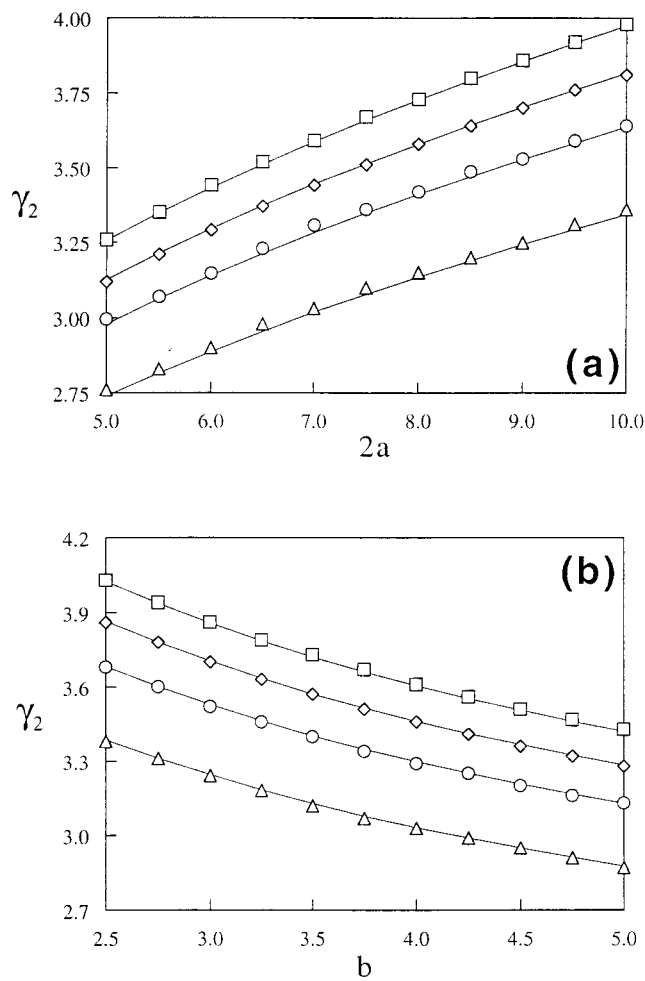
Figure 8. Variation of γ_2 as a function of (a) $2a$ with $b = 5.0$ m and (b) b with $a = 5.0$ m for an elliptic/circular pool with $U_x = 0.5$ m/d (triangles), 0.7 m/d (circles), 0.85 m/d (diamonds) and 1.0 m/d (squares). Symbols represent numerically determined coefficients and solid curves fitted power-law functions.

5. Summary

Local mass transfer correlations describing the rate of the interface mass transfer from single component rectangular or elliptic/circular NAPL pools in saturated, homogeneous porous media are developed. A three-dimensional solute transport model is solved by an ADI, finite difference numerical scheme in order to estimate local mass transfer coefficients for various NAPL pool geometries and hydrodynamic conditions. The aqueous phase concentration of the dissolved solute adjacent to the source is assumed to be equal to the solubility limit. The proposed local mass transfer correlations relate dimensionless local mass transfer
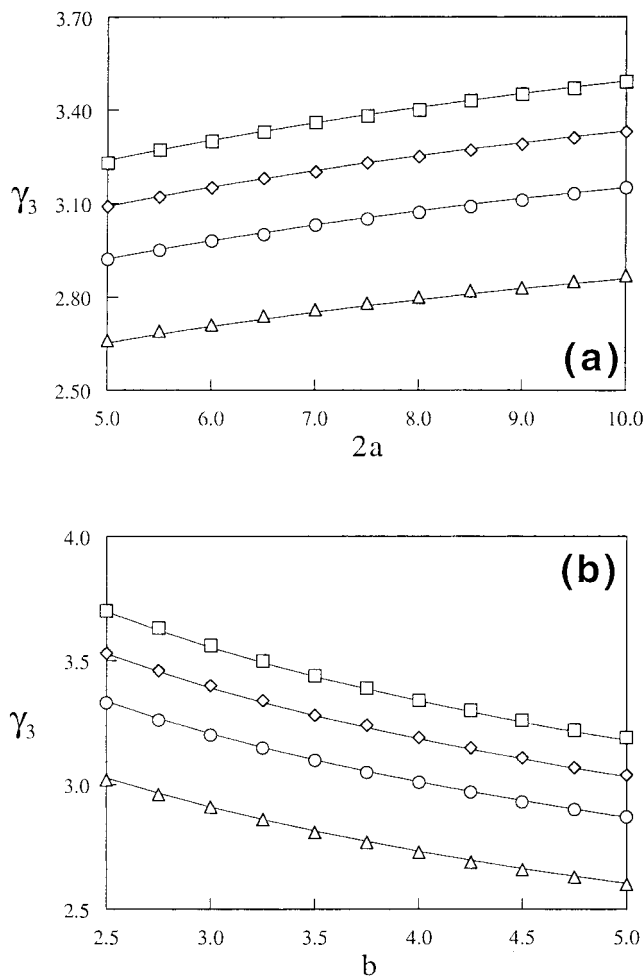
Figure 9. Variation of γ_3 as a function of (a) $2a$ with $b = 5.0$ m and (b) b with $a = 5.0$ m for an elliptic/circular pool with $U_x = 0.5$ m/d (triangles), 0.7 m/d (circles), 0.85 m/d (diamonds) and 1.0 m/d (squares). Symbols represent numerically determined coefficients and solid curves fitted power-law functions.

coefficients (local Sherwood numbers) to appropriate local Peclet numbers. The proposed power-law correlations are fitted to numerically determined local mass transfer coefficients and the associated correlation coefficients are determined by a nonlinear least squares regression method. The correlation coefficients are determined to be functions of the interstitial fluid velocity, pool dimensions and pool geometry. The correlations presented here can be used in existing analytical or numerical mathematical models simulating the transport of dissolved organics originating from the dissolution of NAPL pools in saturated subsurface formations. This work lays the groundwork for future investigations of more realistic situations including complex pool geometries and the presence of dissolving ganglia above the pool affecting the background concentration.

Acknowledgements

References

Anderson, M. R., Johnson, R. L. and Pankow, J. F.: 1992, Dissolution of dense chlorinated solvents into groundwater, 3, Modeling contaminant plumes from fingers and pools of solvent, *Environ. Sci. Tech.* **26**(5), 901–908.

Bear, J. and Verruijt, A.: 1987, *Modeling Groundwater Flow and Pollution,* D. Reidel, Dordrecht.

Bear, J., Ryzhik, V., Braester, C. and Entov, V.: 1996, On the movement of an LNAPL lens on the water table, *Transport in Porous Media* **25**, 283–311.

Bird, R. B., Stewart, W. E. and Lightfoot, E. N.: 1960, *Transport Phenomena*, Wiley.

Borden, R. C. and Kao, C.-M.: 1992, Evaluation of groundwater extraction for remediation of petroleum. Contaminated aquifers, *Water Environ. Res.* **64**(1), 28–36.

Borden, R. C. and Piwoni, M. D.: 1992, Hydrocarbon dissolution and transport–A comparison of equilibrium and kinetic models, *J. Contam. Hydrol.* **10**(4), 309–323.

Celia, M. A., Rajaram, H. and Ferrand, L. A.: 1993, A multi-scale computational model for multiphase flow in porous media, *Adv. Water Resour.* **16**, 81–92.

Chrysikopoulos, C. V.: 1995, Three-dimensional analytical models of contaminant transport from nonaqueous phase liquid pool dissolution in saturated subsurface formations, *Water Resour. Res.* **31**(4), 1137–1145.

Chrysikopoulos, C. V. and Lee, K. Y.: 1998, Contaminant transport resulting from multicomponent nonaqueous phase liquid pool dissolution in three-dimensional subsurface formations, *J. Contam. Hydrol.* **31**, 1–21.

Chrysikopoulos, C. V., Voudrias, E. A. and Fyrillas, M. M.: 1994, Modeling of contaminant transport resulting from dissolution of nonaqueous phase liquid pools in saturated porous media, *Transport in Porous Media* **16**(2), 125–145.

Demond, A. H., Rathfelder, K. and Abriola, L. M.: 1996, Simulation of organic liquid flow in porous media using estimated and measured transport properties, *J. Contam. Hydrol.* **22**, 223–239.

Fried, J. J., Muntzer, P. and Zilliox, L.: 1979, Ground-water pollution by transfer of oil hydrocarbons, *Ground Water* **17**(6), 586–594.

Geller, J. T. and Hunt, J. R.: 1993, Mass transfer from nonaqueous phase organic liquids in water-saturated porous media, *Water Resour. Res.* **29**(4), 833–845.

Hoffman, J. D.: 1992, *Numerical Methods for Engineers and Scientists,* McGraw-Hill.

Holman, H.-Y. N. and Javandel, I.: 1996, Evaluation of transient dissolution of slightly water-soluble compounds from a light nonaqueous phase liquid pool, *Water Resour. Res.* **32**, 915–923.

Huyakorn, P. S., and Pinder, G. F.: 1983, *Computational Methods in Subsurface Flow*, Academic Press, New York.

Illangasekare, T. H., Ramsey Jr., J. L., Jensen, K. H. and Butts, M. B.: 1995, Experimental study of movement and distribution of dense organic contaminants in heterogeneous aquifers, *J. Contam. Hydrol.* **20**, 1–25.

Imhoff, P. T., Jaffé, P. R. and Pinder, G. F.: 1993, An experimental study of complete dissolution of a nonaqueous phase liquid in saturated porous media, *Water Resour. Res.* **30**(2), 307–320.

IMSL: 1991, *IMSL MATH/LIBRARY User's Manual,* ver. 2.0, International Mathematics and Statistics Libraries, Inc., Houston, TX.

Incropera, F. P. and DeWitt, D. P.: 1990, *Fundamentals of Heat and Mass Transfer*, 3rd edn, Wiley, New York.

Johnson, R. L. and Pankow, J. F.: 1992, Dissolution of dense chlorinated solvents into groundwater, 2, Source functions for pools of solvent, *Environ. Sci. Technol.* **26**(5), 896–901.

Keller, A. A., Blunt, M. J. and Roberts, P. V.: 1997, Micromodel observation of the role of oil layers in three-phase flow, *Transort in Porous Media* **26**, 277–297.

Kennedy, C. A. and Lennox, W. C.: 1997, A pore-scale investigation of mass transport from dissolving DNAPL droplets, *J. Contam. Hydrol.* **24**, 221–244.

Lee, K. Y. and Chrysikopoulos, C. V.: 1995, Numerical modeling of three-dimensional contaminant migration from dissolution of multicomponent NAPL pools in saturated porous media, *Environ. Geology* **26**(3), 157–165.

Lee, K. Y. and Chrysikopoulos, C. V.: 1998, NAPL pool dissolution in stratified and anisotropic porous media, *J. Environ. Engng, (ASCE)* **124**(9), 851–862.

Lenhard, R. J., Johnson, T. G. and Parker, J. C.: 1993, Experimental observations of nonaqueous phase liquid subsurface movement, *J. Contam. Hydrol.* **12**, 79–11.

Mackay, D. M., Roberts, P. V. and Cherry, J. A.: 1985, Transport of organic contaminants in groundwater, *Environ. Sci. Technol.* **19**(5), 364–392.

Mason, A. R. and Kueper, B. H.: 1996, Numerical simulation of surfactant-enhanced solubilization of pooled DNAPL, *Environ. Sci. Technol.* **30**, 3205–3215.

Mayer, A. S. and Miller, C. T.: 1996, The influence of mass transfer characteristics and porous media heterogeneity on nonaqueous phase dissolution, *Water Resour. Res.* **32**(6), 1551–1567.

Miller, C. T., Poirier–McNeill, M. M. and Mayer, A. S.: 1990, Dissolution of trapped nonaqueous phase liquids: Mass transfer characteristics, *Water Resour. Res.* **26**(11), 2783–2796.

Parker, J. C., Katyal, A. K., Kaluarachchi, J. J., Lenhard, R. J., Johnson, T. J., Jayaraman, K., Ünlü, K. and Zhu, J. L.: 1991, Modeling multiphase organic chemical transport in soils and groundwater, Final report submitted to U.S. Environmental Protection Agency, Project CR–814320, Washington D.C., U.S.A.

Perry, R. H., Green, D. W. and Maloney, J. O.: 1984, *Perry's Chemical Engineers' Handbook*, 6th edn, McGraw-Hill.

Pinder, G. P. and Abriola, L. M.: 1986, On the simulation of nonaqueous phase organic compounds in the subsurface, *Water Resour. Res.* **22**(9), 109S–119S.

Powers, S. E., Loureiro, C. O., Abriola, L. M. and Weber Jr., W. J.: 1991, Theoretical study of the significance of nonequilibrium dissolution of nonaqueous phase liquids in subsurface systems, *Water Resour. Res.* **27**(4), 463–477.

Powers, S. E., Abriola, L. M. and Weber Jr., W. J.: 1992, An experimental investigation of nonaqueous phase liquid dissolution in saturated subsurface systems: Steady state mass transfer rates, *Water Resour. Res.* **28**(10), 2691–2705.

Schwille, F.: 1975, Groundwater pollution by minimal oil products, *Proc. Moscow Symposium,* AISH Publ. 103, pp. 226–240.

Schwille, F.: 1988, *Dense Chlorinated Solvents in Porous and Fractured Media,* Translated by Pankow, J. F., Lewis Publishers, Inc., Chelsea, Michigan.

Schincariol, R. A., Schwartz, F. W. and Mendoza, C. A.: 1994, On the generation of instabilities in variable density flow, *Water Resour. Res.* **30**(4), 913–927.

Seagren, E. A., Rittmann, B. E. and Valocchi, A. J.: 1993, Quantitative evaluation of flushing and biodegradation for enhancing *in situ* dissolution of nonaqueous-phase liquids, *J. Contam. Hydrol.* **12**, 103–132.

Seagren, E. A., Rittmann, B. E. and Valocchi, A. J.: 1994, Quantitative evaluation of the enhancement of NAPL–pool dissolution by flushing and biodegradation, *Environ. Sci. Technol.* **28**(5), 833–839.

Voudrias, E. A. and Yeh, M. F.: 1994, Dissolution of a toluene pool under constant and variable hydraulic gradient with implications for aquifer remediation, *Ground Water* **32**, 305–311.

Van der Waarden, M., Bridie, A. L. A. M. and Groenewoud, W. M.: 1971, Transport of mineral oil components to groundwater. I. Model experiments on the transfer of hydrocarbons from a residual oil zone to trickling water, *Water Res.* **5**(2), 213–226.

Wang, H. F. and Anderson, M. P.: 1982, *Introduction to Groundwater Modeling*, Academic Press Inc., San Diego, California.

Weber Jr., W. J. and DiGiano, F. A.: 1996, *Process Dynamics in Environmental System*, Wiley.

Wilson, J. T., Conrad, S. H., Hagan, E. and Peplinski, W. R.: 1988, The pore level spatial distribution and saturation of organic liquids in porous media, *Proc. NWWA Conference on Petroleum Hydrocarbons and Organic Chemicals in the Subsurface,* National Well Water Association, Dublin, Ohio, pp. 107–133.